Influence of cooling rate on the precipitation kinetics of nanoscale isothermal ω-phase in metastable β-Ti alloy, Ti–5Al–5Mo–5V–3Cr

Sharma, D., Parfitt, D., Chen, B., Roebuck, B., Venero, D. A., Kada, S. R., Fabijanic, D. & Fitzpatrick, M. E.

Original citation & hyperlink:
Sharma, D, Parfitt, D, Chen, B, Roebuck, B, Venero, DA, Kada, SR, Fabijanic, D & Fitzpatrick, ME 2021, 'Influence of cooling rate on the precipitation kinetics of nanoscale isothermal ω-phase in metastable β-Ti alloy, Ti–5Al–5Mo–5V–3Cr', Journal of Alloys and Compounds, vol. 859, 157822.

DOI 10.1016/j.jallcom.2020.157822
ISSN 0925-8388

Publisher: Elsevier

Influence of cooling rate on the precipitation kinetics of nanoscale isothermal ω-phase in metastable β-Ti alloy, Ti–5Al–5Mo–5V–3Cr

Deepak Sharma[a,b,*], David Parfitt[a], Bo Chen[a,c], Bryan Roebuck[d], Diego Alba Venero[e], Sitarama Raju Kada[b], Daniel Fabijanic[b], Michael E. Fitzpatrick[a]

[a] The Institute for Future Transport and Cities, Coventry University, Coventry, CV1 5FB, UK
[b] The Institute for Frontier Materials, Deakin University, Victoria, 3216, Australia
[c] Department of Engineering, University of Leicester, Leicester, LE1 7RH, UK
[d] National Physical Laboratory, Teddington, London, TW11 0LW, UK
[e] ISIS Neutron and Muon Source, Rutherford Appleton Laboratory, Didcot, Oxfordshire, OX11 0QX, UK

* Corresponding author's e-mail address - sharmad9@uni.coventry.ac.uk; sdeepa@deakin.edu.au

Abstract

In metastable β-Ti alloys, nanoscale isothermal ω-phase (ω_{iso}) precipitates are regarded as the nucleation sites for the α strengthening phase. Here we investigate the precipitation kinetics of the ω_{iso} precipitates as a function of cooling rate (air cooling and water quenching) after β-solutionising. A combined *in situ* small-angle neutron scattering (SANS) and electrical resistivity measurement approach was used during ageing of Ti–5Al–5Mo–5V–3Cr wt% (Ti-5553) alloy at 300 °C and 325 °C up to 8 h. The SANS modelling was consistent with ellipsoid shaped particles for the ω_{iso} precipitates, for both air-cooled and water-quenched samples. The precipitates attained a maximum size (equatorial diameter) of ~21 nm and ~17 nm after 2 h and 4 h of ageing the water-quenched and air-cooled samples respectively. Although the air-cooled samples showed delayed nucleation in comparison to water-quenched sample, the volume fraction became approximately the same (~11 %) after ageing for 8 h. The average value of the activation energy for ω_{iso} nucleation from the β-phase matrix was determined as 122 kJ mol^{-1} from electrical resistivity data using a modified Johnson-Mehl-Avrami-Kolmogorov (JMAK) model. The hardness increased with ageing time, with water quenching leading to a higher final value of hardness than air cooling.

Keywords

Titanium alloys, Kinetics, Small-angle neutron scattering, Electrical resistivity measurements

1. Introduction

The class of metastable β-Ti alloys (e.g. Ti-5553) is considered to be the most versatile in the Ti family [1]. Their ability to offer high specific strength and deeper hardenability has led to their usage in aerospace applications such as landing gear and load-bearing bulkheads [1–3]. These desirable properties are highly dependent on the size, volume fraction, morphology, and the distribution of α-phase precipitates formed in the β-phase matrix [4–6]. The nucleation of the α-phase during thermomechanical processing can occur via two distinct routes: directly from the decomposition of the β-phase through a pseudo-spinodal mechanism [7]; or by nucleation from a precursor ω-phase [8]. The use of the ω-phase-assisted nucleation process may produce a highly refined α-phase distribution, with the potential to significantly improve the alloy strength [9–11]. Hence, it is important to understand the kinetics of ω-phase formation in order to precisely control and optimise the alloy properties.

The metastable β-Ti alloys consist of a body-centred cubic (bcc) β-phase matrix at room temperature that is present after rapid cooling from above the β-transus temperature (T_β). This retention of complete β-phase after solution treatment is due to the presence of a high concentration of slow-diffusing elements such as Mo [2]. An athermal ω-phase (ω_{ath}) is also observed after solution treatment [12]. The ω_{ath} is considered to be formed due to the partial collapse of {111} planes of parent β-phase during rapid cooling [13]. The ω_{ath} evolves to simple hexagonal isothermal ω-phase (ω_{iso}) precipitates at low-temperature (~300 °C) ageing through the diffusion of solute elements allowing the complete collapse of the {111} planes of the β-phase [13]. The hexagonal-close-packed (hcp) α-phase is formed during subsequent higher temperature ageing either homogenously via a pseudo-spinodal decomposition or heterogeneously via ω_{iso} assisted nucleation [2]. An orthorhombic α″-phase is also observed during subsequent ageing at low temperatures (~325°C to 425°C) after either direct quenching to these temperatures, or quenching to room temperature first and subsequently raising the

temperature at a high heating rate [14–16], and a diffusionless process is responsible for the phase formation [17].

Recently, Chen *et al*. [18] reported that the formation of ω_{iso} precipitates during low-temperature (300 °C) ageing is influenced by the cooling rates from the solution treatment temperature of Ti–6Cr–5Mo–5V–4Al β-Ti alloy. Their transmission electron microscopy (TEM) studies qualitatively showed that the number density of ω_{iso} precipitates increased with more rapid cooling. However, an in-depth quantitative understanding of the evolved microstructure is required to precisely control and optimise the mechanical properties. In addition, due to the small volume of the samples, TEM is unable to easily provide statistical information about the path leading to a final desired microstructure. Coakley *et al*. [19] studied the formation of ω_{iso} precipitates in a water-quenched Ti-5553 β-Ti alloy and also quantified the evolved microstructure. However, the effect of different cooling rates such as air cooling on the precipitation kinetics of ω_{iso} precipitates was not studied. Understanding the influence of controlled cooling is highly important for structural applications in the aerospace industry where the section thickness may determine the achievable cooling rate and therefore limit the mechanical properties. Furthermore, these data may help clarify the thermodynamic understanding of the ω_{iso} precipitation from the parent β-phase matrix.

The use of small-angle neutron scattering (SANS) to study precipitate evolution in engineering alloys has gathered considerable attention in the recent past due to its ability to probe the three-dimensional structural information of the material at the nanoscale [19,20]. The SANS technique provides information for a far larger volume of sample than TEM and is still able to probe precipitates of size in the range of 1–100 nm [21,22]. The technique measures the coherent elastic scattering of the incident neutron beam from precipitates at small angles (less than 10°) based on the contrast variation principle, *i.e.* the difference in the scattering length densities (SLD) between the parent phase and precipitate [23].

The formation of ω_{iso} precipitates from the β-phase matrix in Ti alloys has also been detected by means of electrical resistivity [16,24]. This is due to its high sensitivity to the minor constitutional changes in the material during quenching, heating and ageing [25]. This technique is especially interesting due to its capability to derive thermodynamic information such as the activation energy for precipitation [24].

For the current work, samples of Ti-5553 β-Ti alloy produced using air cooling and water quenching after solution treatment were used to establish the influence of the cooling rate on the kinetics of nanoscale ω_{iso} precipitates. *In situ* SANS measurements were used to quantify the evolved microstructure and understand the nucleation and growth kinetics of ω_{iso} precipitates during low-temperature (300 °C) ageing. Complementary *in situ* electrical resistivity measurements conducted during ageing at 300 °C and 325 °C provided additional insight into the precipitation mechanism and activation energy. These *in situ* measurements were supported by conventional scanning electron microscopy (SEM) and X-ray diffraction (XRD) measurements to confirm the phases present. With this combined approach, the kinetics of ω_{iso} precipitates transformation from the β-phase matrix under different cooling rates are clarified. Finally, Vickers microhardness measurements were used to confirm the likely effect of evolved microstructure on the mechanical properties.

2. Experimental details

The Ti-5553 β-Ti alloy used in this work was provided by TIMET in the form of discs of size ø160 mm × 15 mm sectioned from the end of a forged billet. For further usage, samples of size 40 mm × 15 mm × 15 mm were cut from this disc using electrical discharge machining (EDM). These samples were then ground on all sides using 320 grit size SiC abrasive paper to clean the surface, and a Bonderite L-GP Acheson coating was applied to these ground samples to minimise the formation of α-case during solution treatment. After drying the coating for a day, the samples were solution-treated at 900 °C (above T_β~845 °C [26]) for 0.5 h. Two cooling

rates (air cooling and water quenching) were used to cool the samples from above T_β to room temperature, to create the starting microstructure for assessing the effect of cooling rate. The sequence of heat treatment processes is depicted in Fig. 1. The solution heat treatments were performed in a pre-heated tube furnace under argon gas (industrial grade) with a flow rate of 10 l/min. The temperature was maintained within ± 2 °C with the help of a 3 mm diameter N-type thermocouple. The thermocouple was fixed with high-temperature adhesive to a hole drilled at the centre of a reference sample (40 mm × 15 mm × 15 mm). In all solution heat treatment and ageing experiments, a reference sample was placed in the furnace. The cooling rates for air cooling and water quenching were measured as ~0.5 °C/s and ~20 °C/s, respectively.

The selection of the solution heat treatment time and the temperature was intended to provide sufficient homogeneity and was based on previous work where temperatures of 890 °C [27,28], 865 °C [29], and 900 °C [11,31] were used to solution treat the Ti-5553 β-Ti alloy samples for 0.5 h. This is also in accordance with recommended practice [30]. In these studies, variable cooling rates imposed by water, air or gas cooling led to ω_{ath} formation. The formation of α-phase or α″-phase was not reported after these cooling rates – where we have used air cooling and water quenching for our work.

The solution-treated samples were ground on all the sides using 320 grit size SiC abrasive paper to remove any developed α-case, and then samples for SANS (20 mm × 15 mm × ~1 mm), electrical resistivity measurement (matchstick samples: 40 mm × 2 mm × ~1 mm), and samples for subsequent ageing (10 mm × 15 mm × 15 mm) were cut from the solution-treated samples using EDM.

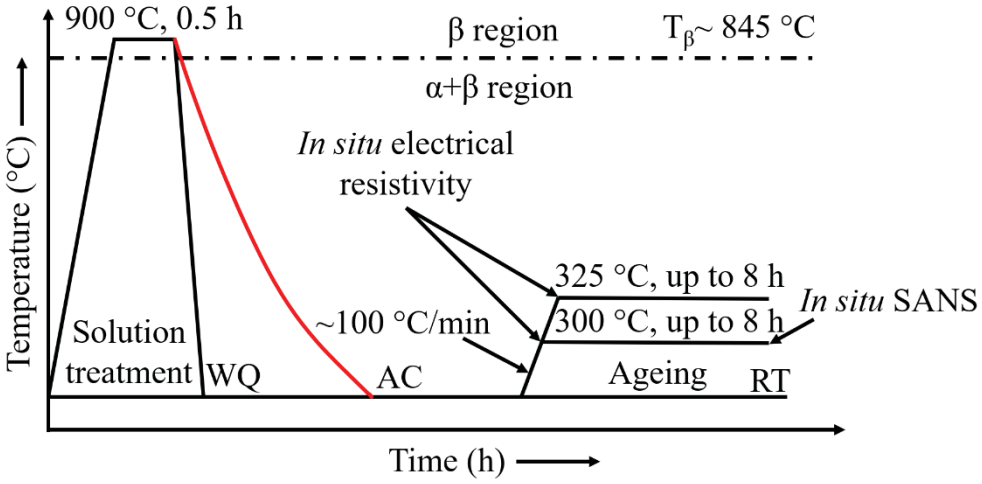

Fig. 1. The schematics of heat treatment cycles used in this work to understand the nucleation and growth kinetics of nanoscale isothermal ω-phase precipitates in Ti-5553 β-Ti alloy as a function of water quenching (WQ) and air cooling (AC) during solution treatment. RT refers to room temperature.

2.1. *In situ* SANS measurements and data reduction

The solution-treated samples were polished up to 1 μm finish using diamond suspension for SANS measurements. The SANS measurements were performed on the LARMOR beamline of the ISIS Pulsed Neutron Source, UK. Polychromatic neutrons (λ = 0.9 to 13.3 Å) were used for measuring the scattering. The detector configuration provided a momentum transfer (q) range of 0.007 – 0.7 Å, where $q = 4\pi\sin\theta/\lambda$ and the scattering angle is 2θ, and λ is the neutron wavelength. The sample scattering was measured by exposing the samples to a neutron beam of cross-section 12 mm × 12 mm. The scattering was measured at room temperature after solution treatment, during heating to the ageing temperature (300 °C), and during ageing at 300 °C up to 8 h, as shown in Fig. 1. Room temperature data were collected first for 60 mins, and then sample temperature was raised to the ageing temperature (300 °C) with a heating rate of ~100 °C/min, and was held for 8 h whilst the measurements were recorded. A K-type thermocouple of diameter 1 mm was attached to the surface of the sample through the sample holder to measure the ageing temperature and the heating rate. The ageing temperature was maintained within ± 2 °C. A radiant air furnace [32] was used for ageing the samples. All the measurements were performed under argon gas atmosphere (industrial grade).

The measured raw SANS data were reduced to absolute SANS intensities (I) using standard procedures in the Mantid software [33]; *i.e.* by correcting the data for transmission and background measurements. The data was azimuthally averaged for plotting the one-dimensional (1D) I vs q plots. For data analysis, the complete 60 min of room temperature data was averaged, but for ageing, the data were combined into 15-minute bins with the exception of 100 s of data averaged immediately after the sample reached the ageing temperature to capture the data at the end of the heating period. An ellipsoid model was used to fit the SANS patterns. This model was chosen based on the understanding of precipitate shape from the literature [34].

2.2. *In situ* electrical resistivity measurement

A miniaturised multi-property test system [35,36] was used to measure the electrical resistivity *in situ* using a 4-point method under an argon atmosphere. The measurements were taken at room temperature, during the heating period, and also during the ageing period at 300 °C or 325 °C for up to 8 h. The temperature profiles of the *in situ* electrical resistivity measurement are also indicated in Fig. 1. These two temperatures were selected based on the temperature of formation of ω_{iso} in Ti-5553 β-Ti alloy [12,26]. In addition, the availability of ageing data at two isothermal conditions is required to derive the activation energy for precipitation based on the modified Johnson-Mehl-Avrami-Kolmogorov (JMAK) model [24]. The measurements were performed on the solution-treated matchstick samples after grinding with 1200 grit SiC abrasive paper. The samples were held between the water-cooled grips, whilst a direct current was used to heat them with a heating rate of ~100 °C/min. The electrical resistivity was measured across the central 2 mm of the sample using a Pt-Rh probe. A Pt/Pt-13%Rh thermocouple with wires having a diameter of 0.1 mm was used to measure the temperature. The thermocouple was spot-welded to the centre of the test sample. The ageing

temperature was maintained within ± 1 °C. The electrical resistivity (ρ) of the samples was calculated using Equation 1

$$\rho = \frac{VA}{Il} \quad (1)$$

where V is the voltage drop, A refers to the cross-sectional area of the sample, I is the current and l refers to the gauge length between potential probes. An increment of ~0.01% in electrical resistivity was estimated due to change in the gauge length during heating that was neglected for further data analysis.

2.3. Ageing treatments

The solution-treated samples after water quenching or air cooling were subsequently aged at 300 °C for a sequence of times (1 h, 2 h, 4 h and 8 h). The ageing was performed in a pre-heated tube furnace under argon gas with a heating rate of ~100 °C/min. Samples were water-quenched after ageing.

2.4. Materials characterisation

The solution-treated and aged samples were metallographically prepared by grinding up to 1200 grit size using SiC abrasive papers followed by sequential polishing using diamond suspension up to 1 µm. Subsequently, vibratory polishing using 0.02 µm particle size colloidal suspension was done to obtain a mirror-like finish. Finally, the samples were cleaned for 0.25 h in an ultrasonic bath using distilled water.

The microstructural features were observed using a Zeiss Gemini Sigma 500VP SEM in backscattered electrons (BSE) mode at an accelerating voltage of 20 kV. XRD phase analysis was performed using CuK_{α} X-ray radiation for a 2θ range of 35° to 100° at a scan rate of 1°/min. The phase identification was done based on the understanding from previously published crystallographic data on Ti alloys [19,20]. Vickers microindentation (0.5 kgf load)

was used to obtain the microhardness of the solution-treated and aged samples. An average of 40 measurements was taken for each sample. The line intercept method in ImageJ software [37] was used to quantify the β-phase grain size (average of 100 measurements reported) for solution-treated samples.

3. Results

3.1. Microstructural characterisation

The BSE-SEM micrographs of samples after water quenching and air cooling exhibited a homogenised microstructure (Fig. 2 (a) and (b) respectively), where the XRD results in Fig. 3 (a) indicating the presence of primarily β-phase in the microstructure. The average β grain size for the water-quenched and the air-cooled samples was measured as 245 ± 75 μm and 225 ± 85 μm, respectively. Note that the presence of an inevitable ω_{ath} (without the size or volume fraction difference) has been reported consistently for the air-cooled and the water-quenched Ti-5553 β-Ti alloy after solution treatment when examined under TEM [11,26,31]. Since the present solution treatment conditions are same as the previous work on the same alloy, it is reasonable to assume the formation of ω_{ath} (undetected by SEM and XRD) in both samples after solution treatment. However, Gao *et al.* [38] reported that air cooling of Ti–7Mo–3Cr–1Fe β-Ti alloy after solution treatment can lead to the increase in the size and volume fraction of the ω-phase when compared to water quenching. Such a difference between the two types of β-Ti alloys, *i.e.* Ti–5Al–5Mo–5V–3Cr and Ti–7Mo–3Cr–1Fe could be due to the role of Fe, because 1 wt% Fe to Ti–7Mo–3Cr β-Ti alloy tailored the formation of ω-phase [38]. Also, the previous TEM studies [11,26,31] did not report any formation of α-phase or α″-phase at room temperature after solution treatment. This is in line with the current XRD observations (Fig. 3 (a)).

The average microhardness values were measured as 300 ± 5 Hv and 298 ± 4 Hv for water-quenched and air-cooled samples, respectively. The BSE-SEM micrographs for the samples aged at 300 °C for 8 h after solution treatment (both water-quenched (Fig. 2 (c)) and air-cooled, Fig. 2 (d))) also showed a homogenised microstructure. However, the presence of a small volume fraction of ω_{iso} precipitates and α″-phase in the β-phase matrix can be inferred in the aged condition from the XRD patterns (Fig. 3 (b)). This is in agreement with the TEM and XRD observations in the literature [16,19] for Ti-5553 β-Ti alloy during ageing.

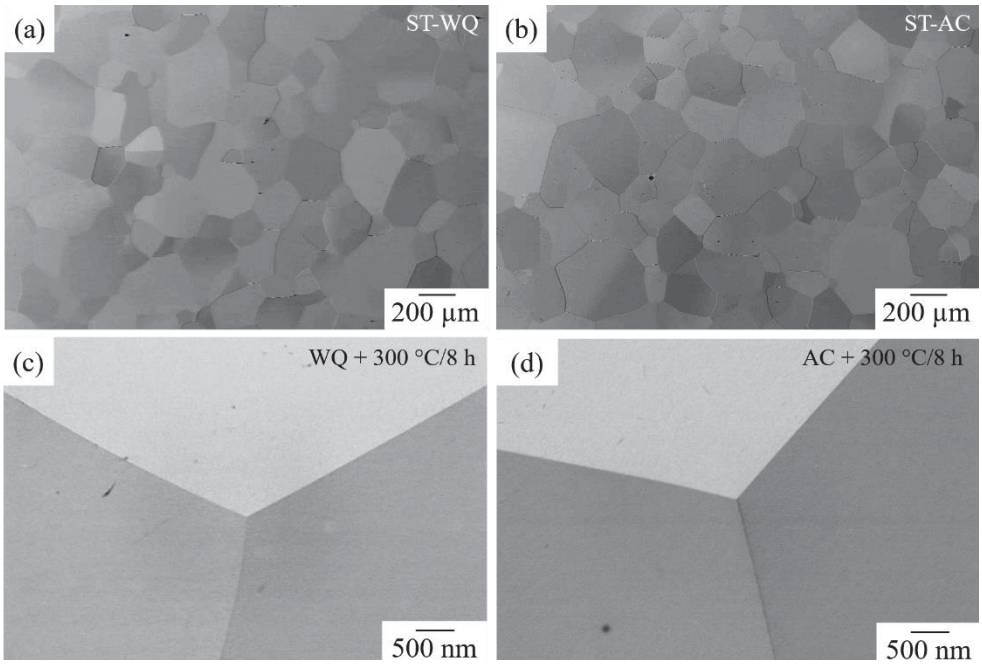

Fig. 2. The BSE-SEM microstructure of Ti-5553 β-Ti alloy samples after solution treatment (ST) using (a) water quenching (WQ) and (b) air cooling (AC). (c) and (d) show the BSE-SEM microstructure of aged samples (300 °C for 8 h) after WQ and AC, respectively.

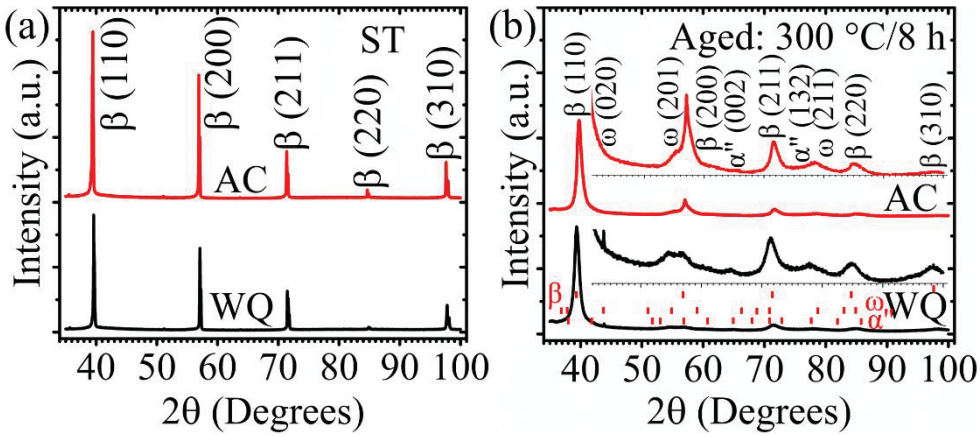

Fig. 3. XRD diffraction patterns of Ti-5553 β-Ti alloy samples after (a) solution treatment (ST) using water quenching (WQ) and air cooling (AC). The XRD patterns show the presence of solely β-phase. The doublets seen in the XRD data are due to the diffraction from both $K\alpha_1$ and $K\alpha_2$ emissions. (b) shows the XRD diffraction patterns after subsequent ageing of the solution-treated samples at 300 °C for 8 h, indicating the presence of β-phase and small volume fraction of isothermal ω-phase and α″-phase. The insets, shown in Fig. (b), are the magnified versions of the XRD patterns. These have been provided to better delineate the data.

3.2. Small-angle neutron scattering

One-dimensional *I* vs *q* plots for all the SANS measurements after water quenching and air cooling are shown in Fig. 4 (a) and (b), respectively. The error bars (~±0.01 cm^{-1}) for each point are not presented in the plots (Fig. 4) to assist in delineating the data. The scattering curves after water quenching and air cooling are significantly different in terms of shape and evolution rate. The scattering curve for the air-cooled sample evolves quite slowly when compared to the water-quenched sample.

The scattering intensity decreased with respect to room temperature scattering when the sample temperature was increased to the ageing temperature (300 °C). This occurred for both cooling rates. During the ageing period, the first additional scattering or deviation from the room temperature scattering was observed after 0.25 h and 1.25 h for water-quenched (at ~0.05 $Å^{-1}$) and air-cooled (at ~0.08 $Å^{-1}$) samples, respectively; for the water-quenched sample the deviation was in agreement with similar SANS measurements obtained by Coakley *et al*. [19]. This additional scattering can be associated with the nucleation of ω_{iso} precipitates [19]. The α″-phase does not affect the SANS signal as observed previously [17] because it is formed by

a diffusionless process [14], creating no contrast difference between the precipitate and the matrix.

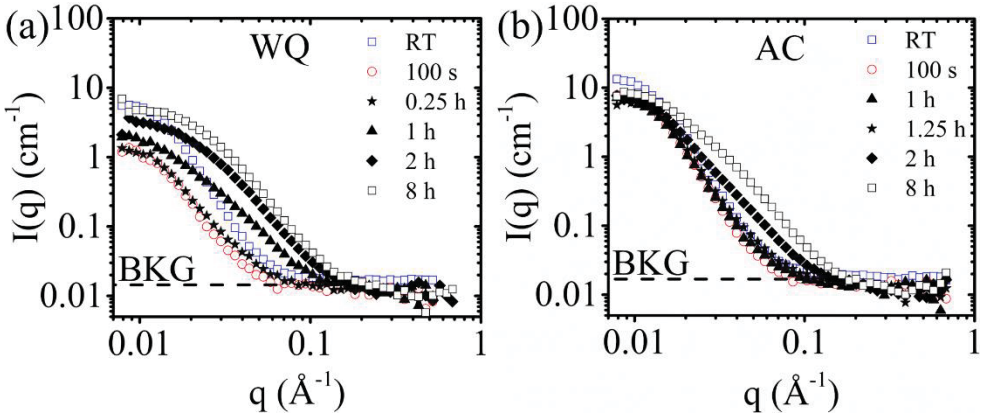

Fig. 4. The one-dimensional intensity (*I*) vs momentum transfer (*q*) plots of SANS scattering for Ti-5553 β-Ti alloy samples measured at room temperature (RT), after initial heating for 100 s, and *in situ* at 300 °C up to 8 h after (a) water quenching (WQ) and (b) air cooling (AC). The times in the legend represent the times at the end of the measurement. BKG refers to the background scattering.

3.3. Electrical resistivity measurements

The electrical resistivity measurements for water-quenched and air-cooled samples were recorded during the entire ageing process, heating from room temperature to 300 °C and 325 °C for up to 8 h. Relative electrical resistivity results are plotted (Fig. 5) to understand the change in the kinetics of ω_{iso} precipitates as a function of cooling rate from the solution treatment temperature (*i.e.* either by water quenching or by air cooling). The solution-treated condition is considered as the reference state in order to calculate the relative electrical resistivity change.

Both air-cooled and water-quenched samples show a similar drop in the electrical resistivity as the temperature was raised to the ageing temperatures (300 °C and 325 °C), as shown in Fig. 5 (a) and (b). This decrease in the electrical resistivity can be associated with the partial dissolution of ω_{ath} [25,39–43].

The evolution of the electrical resistivity during ageing at 300 °C correlates with the kinetics for ω_{iso} formation determined by SANS analysis. The first increase in the electrical

resistivity (discarding the initial drop during the heating period) can be associated with the time to nucleate ω_{iso} precipitates [24]. This occurs for the water-quenched sample (Fig. 5 (c)) after ~0.25 h of ageing, which is consistent with the changes in SANS data that showed a marked increase in scattering between 0.25 and 1 h. In comparison, for the air-cooled sample, the initial increase in electrical resistivity was delayed relative to the water-quenched sample to ~1.25 h. These delayed kinetics are also observed in the scattering intensity derived from the SANS data. After this increase in electrical resistivity during ageing at 300 °C, the electrical resistivity attained an approximate saturation condition after ~5 h and ~6 h of ageing the water-quenched and air-cooled samples, respectively. The formation of α″-phase in Ti-5553 β-Ti alloy happens rapidly after ~2 h of ageing at 325 °C [16]. We did not observe any clear deviation in the electrical resistivity curves (Fig. 5) due to the formation of α″-phase. This is in line with the previous observations [27,28,44], where electrical resistivity measurements were used to examine the precipitation sequences during continuous heating of β-Ti alloys to higher temperatures. The observations from previous research indicate no clear effect of α″-phase early on in the precipitation process and the effect at higher temperatures and longer times is ambiguous and depends upon the alloy composition. We contend therefore that the formation of α″-phase does not affect our early stage kinetics used for subsequent analysis.

For the samples aged at 325 °C, a reduction in the precipitate nucleation time was observed. The first increase in electrical resistivity for the water-quenched sample was observed almost immediately upon reaching the ageing temperature; however, the nucleation time was considerably delayed (~1 h) for the air-cooled sample. As for the samples measured at 300 °C, the electrical resistivity increased further (Fig. 5 (d)) and attained an approximate saturation condition after ~3 h and ~5 h of ageing the water-quenched and air-cooled samples, respectively.

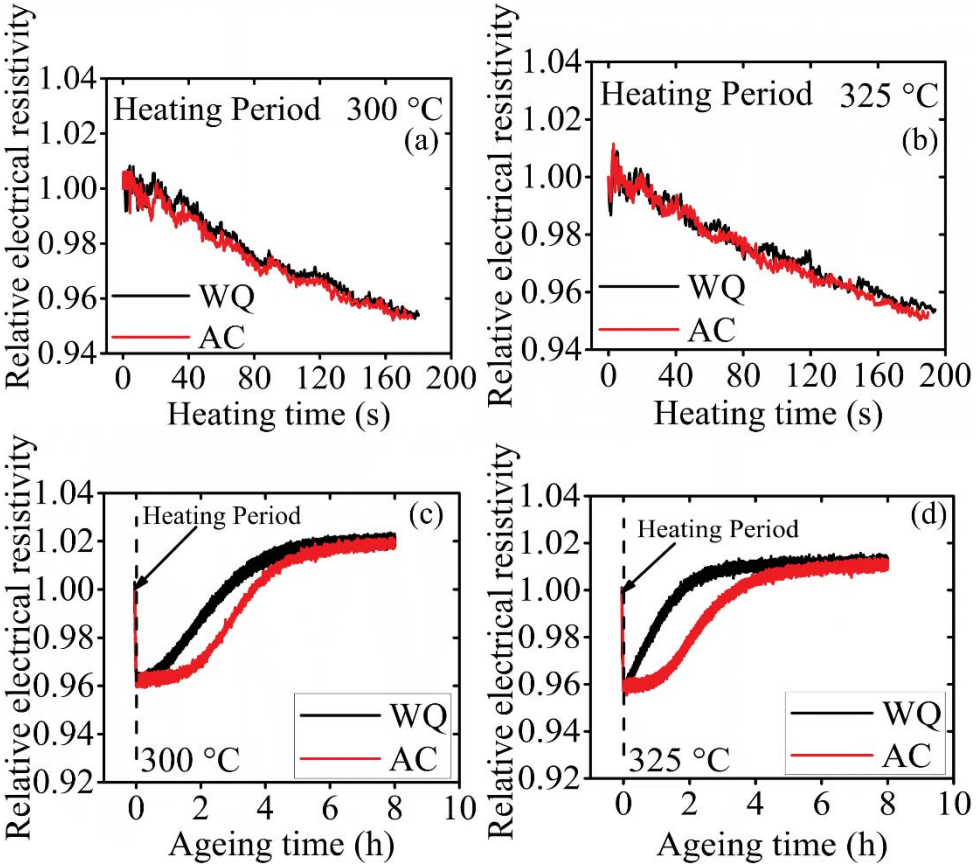

Fig. 5. The evolution of electrical resistivity measurements for Ti-5553 β-Ti alloy recorded *in situ* at room temperature, heating period to reach (a) 300 °C and (b) 325 °C, and during ageing at (c) 300 °C and (d) 325 °C up to 8 h.

3.4. Microhardness

The evolution of Vickers microhardness for the solution-treated and the aged alloy is shown in Fig. 6. The figure also shows the comparison of the microhardness values for the current work with the literature [19,31] on water-quenched Ti-5553 β-Ti alloy. The water-quenched samples showed higher hardness after ageing when compared to the air-cooled samples. The obtained microhardness values for the current work are on the higher side when compared to the literature, as shown in Fig. 6. This additional increment in the hardness with respect to the literature values could be due to the presence of α″. The increment in the hardness by α″ is also dependent on its volume fraction in the matrix [45].

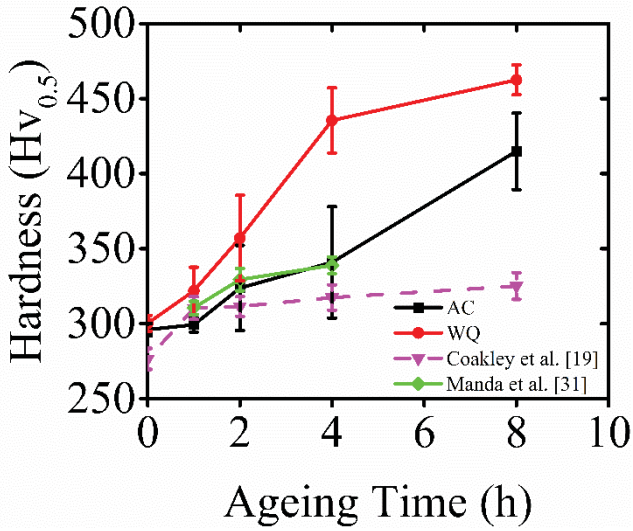

Fig. 6. The characteristic evolution of Vickers microhardness for Ti-5553 β-Ti alloy as a function of ageing time up to 8 h at 300 °C. The plot also shows the comparison of microhardness values obtained for the current work with the available values in the literature for the same alloy after water quenching at same ageing conditions.

4. Discussion

4.1. Interpretation of SANS measurements

Although the SEM images showed a homogenised microstructure at room temperature, the solution-treated samples presented a SANS signal, shown in Fig 7, that can be described by Guinier and Porod regions, labelled as region I and region II respectively. The SANS signals after the heating period (100 s of ageing data) can also be divided into similar regimes. The Porod regime exhibits q^{-4} behaviour (region II). The exponent –4 is related to the smooth interface of the precipitates and the matrix [23,46]. However, the Guinier regime (region I) shows an exponent value of zero. The Guinier regime is related to the real space regions of size $> q^{-1}$ *i.e.* regions much greater than the precipitates size. As explained in section 3.1, the inevitable ω_{ath} must be present in the solution-treated condition for metastable β-Ti alloys after water quenching and air cooling [18,26]. Thus, the scattering observed from region II at room temperature can be associated with the interfaces of ω_{ath} and β-phase matrix [13,19,40]; although, there was no obvious scattering from the ω_{ath} precipitates themselves. This can be due to the fact that ω_{ath} and β-phases have the same composition [17].

The interpretation of these data is similar to the observation of Coakley *et al*. [19] where they did not report any scattering from ω_{ath} in their SANS measurement work on water-quenched Ti-5553 β-Ti alloy samples. However, they did observe the similar *I* vs *q* trend at room temperature. In addition, they did not observe any scattering from the Guinier regime (region I), though this may be due to the reduced *q* range used (~0.01– 0.3 Å). It is also important to note here that the intensity of scattering decreased as the temperature was raised from room temperature to the ageing temperature (300 °C). This was not observed by Coakley *et al*. [19]. The drop in the intensity was much pronounced in the water-quenched sample (Fig. 7 (a)) than the air-cooled sample (Fig. 7 (b)). The scattering curves in region II at room temperature and after heating seem to have the same slope, but there are deviations in region I for water-quenched and air-cooled samples, respectively, with a more significant deviation for the water-quenched material. We attribute this reduction of the SANS intensity to a homogenisation process of the partially resolved large scattering features as scattering is coming from Guinier regime. Since the aim of this paper is to investigate the creation and evolution of the ω_{iso} precipitates, we will assume that once the large scattering features have been dissolved into the matrix then this contribution will remain constant during the thermal treatment and that the variations on the SANS are originated by the ω_{iso} precipitates.

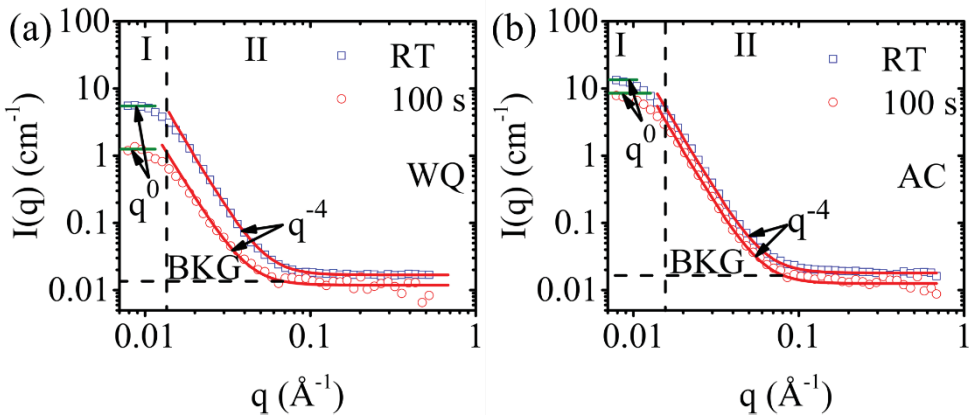

Fig. 7. One-dimensional plots of scattering intensity (I) vs scattering vector (q) for SANS measurements for Ti-5553 β-Ti alloy at room temperature (RT) and after the heating period (100 s of ageing data at 300 °C) after (a) water quenching (WQ) and (b) air cooling (AC) during solution treatment.

The SANS data collected for the aged samples can also be divided into Guinier and Porod regions; however, as the sample ages, the I vs q decay at intermediate q values showed a deviation from the Guinier and Porod regime which indicated the scattering coming from the precipitates [46].

4.2. Model fitting of SANS data

For model fitting of a monodisperse system having Guinier and Porod regions, the SANS intensity (I) is given by Equation 2

$$I(q) = NV^2(\Delta\rho)^2P(q)S(q) + aq^{-4} + be^{\left[\frac{-q^2+R_g^2}{3}\right]} + BKG \quad (2)$$

where N refers to the number density of the precipitates per unit volume, V defines the volume of a single particle, $\Delta\rho$ defines the contrast (SLD) difference between the precipitate and the matrix, $P(q)$ is the particle shape function and BKG refers to an incoherent background scattering that is not desirable for data reduction [46]. $P(q)$ can be further defined in terms of form factors depending on the shape of the precipitates, as given in Equation 3. The form factor for ellipsoid shape precipitates (the model used in this work) has been described in Equation 4. $S(q)$ refers to the structure factor that incorporates the interparticle interference. A hard sphere model was considered in the current work, as recommended in [20], where $S(q)$ can be further

defined as Equation 6. The scattering from the Guinier and Porod regions can be described by $be^{[\frac{-q^2+R_g^2}{3}]}$ and aq^{-4} respectively [47], where a and b are the scale factors for model fitting. R_g refers to the radius of gyration indicating the characteristic size factor for the Guinier region.

$$P(q) = \int_0^\infty F(q,r)^2 dr \tag{3}$$

$$F_{\text{ellipsoid}}(q,r) = 3\frac{(\sin(qr) - qr\cos(qr))}{(qr)^3} \tag{4}$$

where r can be obtained from Equation (5)

$$r = [R_e^2 \sin^2\alpha + R_p^2 \cos^2\alpha]^{0.5} \tag{5}$$

R_e and R_p refer to the equatorial and polar radii perpendicular and along the rotational axis of the ellipsoid respectively, whilst α represents the angle between the axis of the ellipsoid and q.

$$S(q) = \frac{1}{(1-C(q))} \tag{6}$$

$C(q)$ can be defined in terms of volume fraction V_{HS} and diameter (D) of the hard spheres, as described in Equation (7)

$$C(q) = -\frac{24V_{HS}}{(qD)^6}[\beta(qD)^3(\sin qD - qD\cos qD) + \gamma(qD)^2\{2qD\sin qD - (q^2D^2 - 2)\cos qD - 2\} + \delta\{(4q^3D^3 - 24qD)\sin qD - (q^4D^4 - 12q^2D^2 + 24)\cos qD + 24\}] \tag{7}$$

where β, γ and δ can be defined by Equation (8), (9) and (10) respectively.

$$\beta = \frac{(1+2V_{HS})^2}{(1-V_{HS})^4} \tag{8}$$

$$\gamma = -6V_{HS}\frac{(1+\frac{V_{HS}}{2})^2}{(1-V_{HS})^4} \tag{9}$$

$$\delta = \frac{1}{2}V_{HS}\frac{(1+2V_{HS})^2}{(1-V_{HS})^4} \tag{10}$$

The model fitting of the SANS data was undertaken in SASView software [47] to determine the real-space precipitate size. Based on the understanding from the literature [19,34], both disc and ellipsoid shape model fittings were considered for the SANS measurements. However, the ellipsoid shape model fitting provided better fit, which was determined based on the residuals and Chi-squared values. Curve fitting applied to the experimental data was performed by maintaining contrast values for ω_{iso} precipitates ($\rho_\omega = -1.7 \times 10^{10}$ cm^{-2}) and the β-phase matrix ($\rho_\beta = -1.3 \times 10^{10}$ cm^{-2}), as obtained by Coakley *et al*. [19]. The R_g values for the Guinier region were calculated first using the Kratky plots [46]. These values were held constant during the model refinement as shown in Equation 2. The predicted evolution of the ω_{iso} precipitate size and volume fraction parameters during ageing is shown in Fig. 8 and 9, respectively.

It can be seen from Fig. 8 that the ω_{iso} precipitates attained an approximate maximum stable polar radius (R_p) after ~1 h and ~3 h of ageing at 300 °C in the water-quenched and air-cooled samples, respectively. However, the equatorial radius (R_e) became approximately constant after 2 h and 4 h of ageing the water-quenched and air-cooled samples, respectively, indicating that an approximately stable size was attained. The formation of a stable size of ω_{iso} precipitates after 2 h of ageing was also observed by Coakley *et al*. [48] during ageing of water-quenched Ti-5553 β-Ti alloy. It could also be observed from Fig. 8 that the polar dimension attained a stable size earlier than the equatorial radius. This may be due to the higher strain field at the ω_{iso}/β interface, which leads to the preferential growth in <111> β directions, as reported by Sun *et al*. [24]. The SANS model-fitted dimensions of ω_{iso} precipitates along the equatorial dimensions (~ 21 nm diameter) after 8 h ageing the water-quenched sample lies in the range of TEM observations (~10–50 nm) reported in the literature [34].

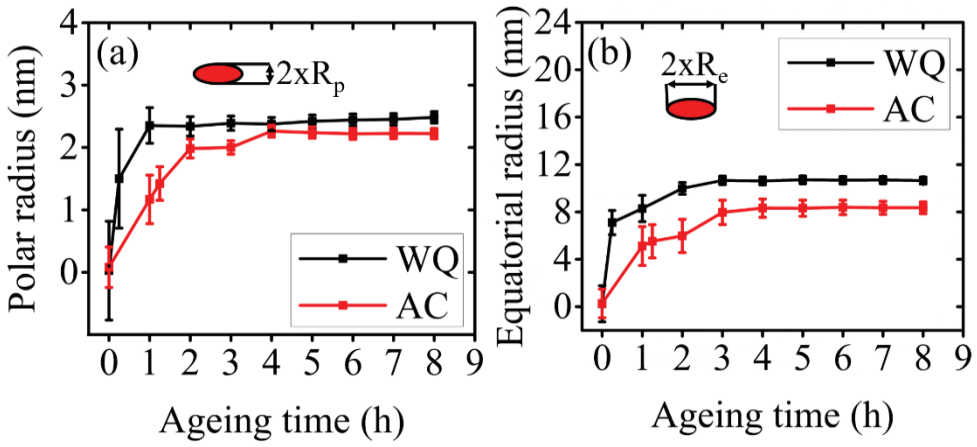

Fig. 8. The evolution of isothermal ω-phase precipitate during the ageing time at 300 °C up to 8 h after water quenching (WQ) and air cooling (AC). (a) shows the characteristic polar size of the precipitates, whilst (b) shows the evolution in the equatorial dimension of the precipitate.

The characteristic evolution of the volume fraction of ω_{iso} precipitates obtained from the ellipsoid model fitting is shown in Fig. 9. The volume fraction increased with ageing time. Both the samples (water-quenched and air-cooled) showed approximately similar volume fraction (~11 %) after 8 h of ageing at 300 °C. This is in agreement with the observations of Coakley *et al*. [19] with a reported volume fraction of ~10 % for the water-quenched Ti-5553 β-Ti alloy in a similar ageing condition. The qualitative understanding of Chen *et al*. [18] based on their TEM observation, showed that the faster cooling rate increases the number density of ω_{iso} precipitates. However, from the current observations, it is stated that the delayed nucleation does happen with the slow cooling rate, but approximately the same volume fraction is observed once the saturation stage is reached.

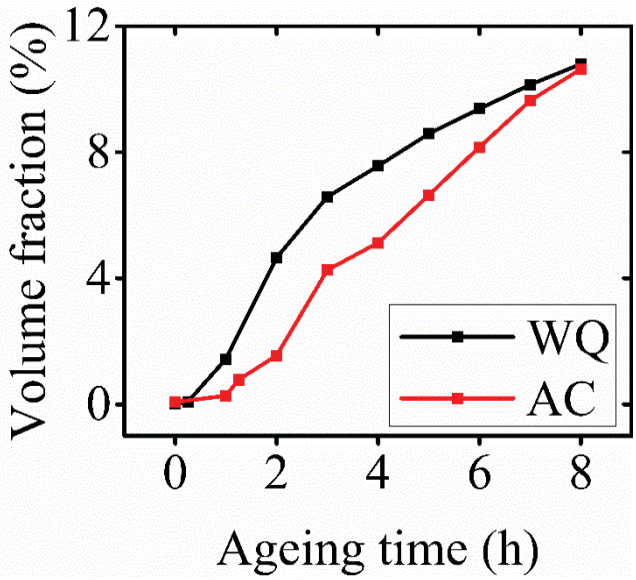

Fig. 9. The characteristic evolution of volume fraction of isothermal ω-phase precipitates obtained from the ellipsoid model fitting. It could be seen from the plot that the volume fraction increased as a function of ageing time.

4.3. Analysis of initial trends upon heating

Upon heating, there is a drop in the electrical resistivity of both the air-cooled and water-quenched samples. This initial drop in the electrical resistivity can be associated with the partial disappearance of ω_{ath} as seen previously [39–41]. This drop is of similar magnitude and rate (Fig. 5 (a)). Therefore, it is reasonable to assume that the volume fraction of ω_{ath} is approximately similar between both the samples at room temperature and are unaffected by the cooling rate difference for Ti-5553 β-Ti alloy. This could also be confirmed from similar microhardness values after solution treatment for both cooling rates. It is also important to note that the β grain size remained approximately the same.

Upon heating, the SANS data also show a drop in total scattered intensity. The observed decay of the SANS signal in the initial stages of the thermal treatment is different in both samples. The reduction in the air-cooled sample is smaller than the one observed in the water-quenched sample. Our interpretation of this effect is that the large scattering features formed during the initial cooling process is related to the cooling rate: A slower cooling rate will produce a much more stable volume fraction of these features (Fig. 7 (b)). This could be

attributed to the fact that slower cooling has allowed diffusion to happen that has provided an ageing effect leading to the higher degree of solute partitioning for the air-cooled sample, as observed by Chen *et al*. [18].

4.4. Effect of cooling rate on isothermal ω-phase precipitation

4.4.1. Transformed fraction

The transformed fraction (F) of ω_{iso} precipitates obtained from electrical resistivity measurements during ageing at 300 °C and 325 °C are presented in Fig. 10. The transformed fraction represents the ratio between the volume fraction of ω_{iso} precipitates at time t during ageing and the volume fraction formed at the metastable equilibrium state [49,50] and is given by Equation 11

$$F = \frac{\rho_t - \rho_0}{\rho_{meta} - \rho_0} \tag{11}$$

where ρ_t refers to the electrical resistivity of the alloy at time t during the ageing period, ρ_0 refers to the electrical resistivity of the alloy at the beginning of ageing, and ρ_{meta} refers to the electrical resistivity of the alloy at the end of the ageing time.

The electrical resistivity results (Fig. 5) show that the water-quenched and air-cooled samples exhibited similar trends, but the air-cooled samples showed a delay in the nucleation of the ω_{iso} precipitates (Fig. 10). Also, the nucleation behaviour showed transient nucleation kinetics for both the cases: *i.e*., an incubation time (τ) is required to reach the critical nucleation size. This early nucleation in the water-quenched sample could be attributed to the higher dislocation density in the sample [49]. In addition, Chen *et al*. [48] reported that an air-cooled sample has shown a higher degree of solute partitioning due to the ageing effect during air cooling. This would make the β-phase matrix of the air-cooled sample more stable at room temperature, and a higher amount of energy would be required during ageing for separation of other phases from the stable matrix. This could be another reason for the delay in the nucleation

of the ω_{iso} precipitates in the air-cooled sample, as observed in SANS (Fig. 9) and electrical resistivity data (Fig. 10). The obtained trend at the beginning of the transformed fraction (Fig. 10) correlates to the evolution trend of ω_{iso} volume fraction obtained from SANS data fitting (Fig. 9). However, the electrical resistivity data (Fig. 10) shows a transformed fraction of ω_{iso} precipitates that almost saturates between 4–6 h of ageing, whilst the volume fraction obtained from SANS data (Fig. 9) showed an increasing trend even after reaching 6 h of ageing time. The intensity of the SANS signals is directly dependent on the volume fraction of the precipitates or the difference in the SLD values of the precipitate and the matrix phase (see Equation 2). As indicated by Equation 2, a slight variation in the SLD values or the volume fraction will cause the change in the scattering intensity of the SANS signals. In the present work, the SLD is held constant during refinement. However, it is possible that the SLD values of the precipitates and the matrix phase will evolve during the ageing as the formation of isothermal ω-phase happens by a diffusional process, leading to a slight change in the calculated volume fraction of ω_{iso} precipitates. It is important to note here that the initial trends for ω_{iso} evolution obtained from SANS (Fig. 9) and electrical resistivity data (Fig. 10) matches qualitatively.

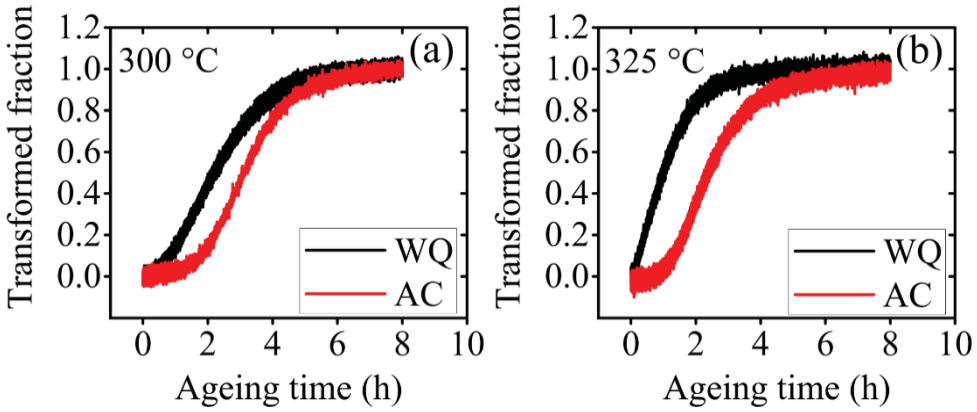

Fig. 10. Kinetic curves showing the ω_{iso} transformed fraction vs. ageing time: at (a) 300 °C and (b) 325 °C. The air-cooled samples showed a delayed nucleation of ω_{iso} precipitates.

4.4.2. Precipitation mechanism

The universal Johnson-Mehl-Avrami-Kolmogorov (JMAK) model can be used to understand the isothermal transformation kinetics under specific assumptions [51]. However, the transient nucleation as observed from the transformed fraction (Fig. 10) violates the universal JMAK model [51,52]. Hence, a modified JMAK model was used to understand the isothermal transformation kinetics of ω_{iso} precipitates. The modified JMAK model [24,45] is given by Equation 12

$$F(t) = 1 - \exp\left(-K_T(t-\tau)^m\right) \tag{12}$$

$$K_T = k_0 e^{-E_a/RT} \tag{13}$$

where m represents the Avrami exponent which is indicative of the precipitation mechanism, K_T is the thermally activated rate constant dependent on the nucleation and growth rate. This can be determined from the Arrhenius relation (Equation (13)), where E_a is the activation energy, R is the universal gas constant and T is the absolute temperature of isothermal ageing. τ refers to the incubation time required to achieve a steady-state precipitate size.

The Avrami exponent, m, was determined over the full range of ω_{iso} precipitation at 300 °C and 325 °C using Equation (14) and the gradients are shown in Fig. 11.

$$ln[-ln(1-F)] = lnK_T + mln(t-\tau) \tag{14}$$

The τ values obtained for water-quenched and air-cooled samples are ~0.25 h and ~1.25 h, respectively. An m value of approximately 1.35 (see Fig. 11) was obtained at the early stage of transformation. These Avrami exponent values can be used to interpret the precipitation mechanism in the material. The transformation initiated by homogenous transient nucleation is often characterised by an Avrami exponent m of greater than 4, whilst for heterogenous transient nucleation, the m tends to be less than 4 [51]. Hence, m value of approximately 1.35,

as determined from Fig. 11, is indicative of a predominant growth mechanism from a pre-existing nucleation site [24,51]. This is in line with the growth of ω_{iso} precipitates from ω_{ath} [13]. However, the m values reduced at later stage of transformation (Fig. 11 and Table 1). This reduction in the m values has been attributed to the dimension loss for ω_{iso} precipitates at later stages of precipitation due to high misfit strain at the ω_{iso}/β interface [24]. This can also be confirmed with the SANS measurement results during the early stage of transformation (Fig. 8). For water-quenched and air-cooled samples during ageing at 300 °C, the deviations in m values were observed after ~40% and ~60% of transformation (Fig. 11), respectively. This is in reasonable agreement with the SANS observations (Fig. 8), where an approximate stable size of ω_{iso} precipitates was achieved during ageing time between 1–2 h for the water-quenched sample (~40% of transformation) and 2–4 h for the air-cooled sample (~60% of transformation) after growth along the major axis.

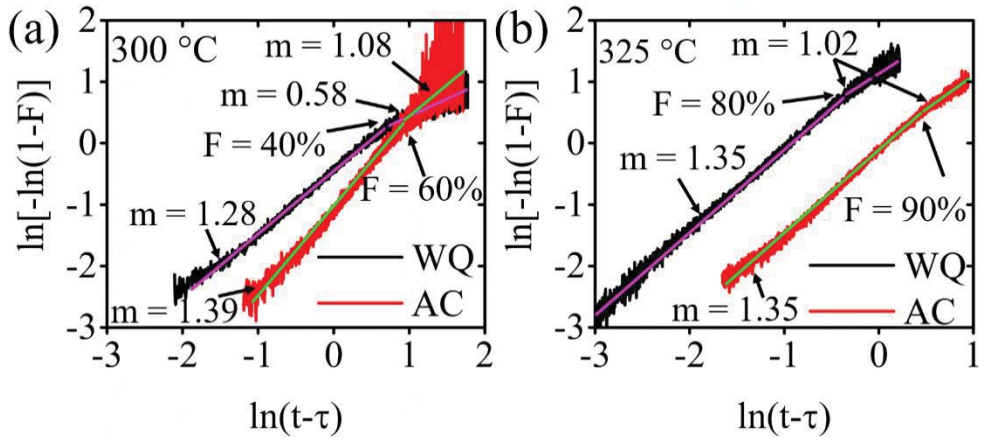

Fig. 11. The modified JMAK plots for Avrami exponents (m) during isothermal ω-phase transformation for the water-quenched (WQ) and air-cooled (AC) samples at (a) 300 and (b) 325 °C.

The analysis of the electrical resistivity measurements using the modified JMAK model indicates that the activation energy (E_a) for the formation of ω_{iso} in the air-cooled sample is higher than in the water-quenched sample (Table 1). Hence, this can assist in rationalising the increased incubation time (τ) for ω_{iso} nucleation in the air-cooled sample as compared to the water-quenched sample (Fig. 10). The average value of the activation energy for the formation

of ω_{iso} precipitates from the β-phase matrix was calculated as ~122 kJ mol^{-1}. This value is in agreement with the activation energy for the diffusion of Mo atoms in the Ti substrate (~135 kJ mol^{-1}) [53]. Being the slowest diffusing element [54] in the current alloy indicates that the formation of ω_{iso} precipitates is controlled by the diffusion rate of Mo, as reported earlier [55]. This is good evidence to state that the electrical resistivity is able to pick up the β to ω_{iso} precipitates transformation. The observance of similar trends via electrical resistivity measurements and SANS measurements indicates the same transformation, *i.e.* β to ω_{iso} precipitates transformation.

Table. 1. The Avrami exponent (m) and activation energy (E_a) values for entire nanoscale ω_{iso} precipitate transformation following water quenching (WQ) and air cooling (AC) during ageing at 300 °C and 325 °C up to 8 h.

	Temperature / °C	Early stage transformation			Later stage transformation
		n (±0.05)	K_T ($\times 10^{-3}$)	E_a (±12 kJ mol^{-1})	n (±0.05)
WQ	300	1.28	16.84	114	0.58
	325	1.35	45.78		1.02
AC	300	1.39	3.18	131	1.08
	325	1.35	10.05		1.02

Conclusions

A combination of *in situ* small-angle neutron scattering (SANS) and electrical resistivity measurement techniques was used to study the kinetics of isothermal ω-phase (ω_{iso}) precipitates during isothermal ageing at 300 °C and 325 °C up to 8 h as a function of different cooling rates (water quenching and air cooling) from solution treatment temperature. The following conclusions can be drawn:

1. A delayed nucleation of ω_{iso} precipitates was observed for air-cooled sample during ageing at 300 °C as compared to water-quenched sample.

2. Although the air-cooled samples showed a delayed nucleation in comparison to water-quenched sample, the volume fraction became approximately the same (~11 %) after ageing for 8 h.
3. From SANS observations, the ellipsoidal ω_{iso} precipitates achieved a maximum size (equatorial diameter = ~21 nm and ~17 nm) after 2 h and 4 h of ageing the water-quenched and air-cooled samples, respectively.
4. The Avrami exponent decreased at higher transformed fraction indicating that the growth of the ω_{iso} precipitates is restricted on one dimension only due to the high misfit strain at β/ω interface. This is in line with the SANS observations where only the equatorial dimension of ω_{iso} precipitates grew at later stages of transformation before achieving the maximum size.
5. The Vickers microhardness results showed an increasing trend with ageing time, where water-quenched samples showed higher hardness compared to air-cooled samples.

Acknowledgements

MEF is grateful for funding from the Lloyd's Register Foundation (LRF), a charitable foundation helping to protect life and property by supporting engineering-related education, public engagement and the application of research. BC acknowledges financial supports by the UK's Engineering and Physical Sciences Research Council, EPSRC Early Career Fellowship Scheme EP/R043973/1. DS would like to thank Prof. Matthew Robert Barnett (Director, The Institute for Frontier Materials, Deakin University, Australia) for his valuable suggestions on SANS and electrical resistivity data. DS is also grateful to Dr. Yiqiang Wang (Senior Materials Engineer, CCFE, UK Atomic Energy Authority) for the fruitful discussions on SANS modelling. The authors are grateful to the ISIS Pulsed Neutron and Muon Source, UK for allowing the use of the LARMOR beamline via RB 1820495.

References

[1] P.J. Bania, Beta titanium alloys and their role in the titanium industry, JOM, (1994) 16–19. doi:10.1007/BF03220742.

[2] G. Lütjering, J.C. Williams, Titanium, Second ed., Springer, New York, 2007.

[3] R.R. Boyer, An overview on the use of titanium in the aerospace industry, Mater. Sci. Eng. A. 213 (1996) 103–114. doi:10.1016/0921-5093(96)10233-1.

[4] O.M. Ivasishin, P.E. Markovsky, S.L. Semiatin, C.H. Ward, Aging response of coarse- and fine-grained β titanium alloys, Mater. Sci. Eng. A. 405 (2005) 296–305. doi:10.1016/j.msea.2005.06.027.

[5] Y. Chen, Z. Du, S. Xiao, L. Xu, J. Tian, Effect of aging heat treatment on microstructure and tensile properties of a new β high strength titanium alloy, J. Alloys Compd. 586 (2014) 588–592. doi:10.1016/j.jallcom.2013.10.096.

[6] J. Fan, J. Li, H. Kou, K. Hua, B. Tang, Y. Zhang, Microstructure and mechanical property correlation and property optimization of a near β titanium alloy Ti-7333, J. Alloys Compd. 682 (2016) 517–524. doi:10.1016/j.jallcom.2016.04.303.

[7] S. Nag, Y. Zheng, R.E.A. Williams, A. Devaraj, A. Boyne, Y. Wang *et al.*, Non-classical homogeneous precipitation mediated by compositional fluctuations in titanium alloys, Acta Mater. 60 (2012) 6247–6256. doi:10.1016/j.actamat.2012.07.033.

[8] S. Nag, R. Banerjee, R. Srinivasan, J.Y. Hwang, M. Harper, H.L. Fraser, ω-Assisted nucleation and growth of α precipitates in the Ti-5Al-5Mo-5V-3Cr-0.5Fe β titanium alloy, Acta Mater. 57 (2009) 2136–2147. doi:10.1016/j.actamat.2009.01.007.

[9] Y. Zheng, R.E.A. Williams, D. Wang, R. Shi, S. Nag, P. Kami *et al.*, Role of ω phase in the formation of extremely refined intragranular α precipitates in metastable β-titanium alloys, Acta Mater. 103 (2016) 850–858. doi:10.1016/j.actamat.2015.11.020.

[10] R. Santhosh, M. Geetha, V.K. Saxena, M. Nageswararao, Studies on single and duplex aging of metastable beta titanium alloy Ti-15V-3Cr-3Al-3Sn, J. Alloys Compd. 605 (2014) 222–229. doi:10.1016/j.jallcom.2014.03.183.

[11] L. Ren, W. Xiao, W. Han, C. Ma, L. Zhou, Influence of duplex ageing on secondary α precipitates and mechanical properties of the near β -Ti alloy Ti-55531, Mater. Charact. 144 (2018) 1–8. doi:10.1016/j.matchar.2018.06.025.

[12] N.G. Jones, R.J. Dashwood, M. Jackson, D. Dye, β Phase decomposition in Ti-5Al-5Mo-5V-3Cr, Acta Mater. 57 (2009) 3830–3839. doi:10.1016/j.actamat.2009.04.031.

[13] S. Nag, A. Devaraj, R. Srinivasan, R.E.A. Williams, N. Gupta, G.B. Viswanathan *et al.*, Novel mixed-mode phase transition involving a composition-dependent displacive component, Phys. Rev. Lett. 106 (2011) 7–10. doi:10.1103/PhysRevLett.106.245701.

[14] A. Settefrati, E. Aeby-Gautier, B. Appolaire, M. Dehmas, G. Geandier, G. Khelifati, Low temperature transformations in β-metastable Ti 5553 titanium alloy, Mater. Sci. Forum. 738–739 (2013) 97–102. doi:10.4028/www.scientific.net/MSF.738-739.97.

[15] A. Settefrati, M. Dehmas, G. Geandier, B. Denand, E. Aeby-Gautier, B. Appolaire *et al.*, Precipitation sequences in beta metastable phase of Ti-5553 alloy during ageing, Proc. 12th World Conf. Titan. (2011) 468–472.

[16] E. Aeby-Gautier, A. Settefrati, F. Bruneseaux, B. Appolaire, B. Denand, M. Dehmas *et al.*, Isothermal α″ formation in β metastable titanium alloys, J. Alloys Compd. 577 (2013) S439–S443. doi:10.1016/j.jallcom.2012.02.046.

[17] J. Coakley, B.S. Seong, D. Dye, M. Ohnuma, Isothermal omega kinetics in beta-titanium alloys, Philos. Mag. Lett. 97 (2017) 83–91. doi:10.1080/09500839.2017.1282633.

[18] J. Chen, W. Xiao, M.S. Dargusch, C. Ma, The dependence of isothermal ω precipitation on the quenching rate in a metastable β-Ti alloy, Sci. Rep. 5 (2015) 1–6. doi:10.1038/srep14632.

[19] J. Coakley, V.A. Vorontsov, N.G. Jones, A. Radecka, P.A.J. Bagot, K.C. Littrell *et al.*, Precipitation processes in the beta-titanium alloy Ti-5Al-5Mo-5V-3Cr, J. Alloys Compd. 646 (2015) 946–953. doi:10.1016/j.jallcom.2015.05.251.

[20] J. Coakley, V.A. Vorontsov, K.C. Littrell, R.K. Heenan, M. Ohnuma, N.G. Jones *et al.*, Nanoprecipitation in a beta-titanium alloy, J. Alloys Compd. 623 (2015) 146–156. doi:10.1016/j.jallcom.2014.10.038.

[21] F. De Geuser, A. Deschamps, Precipitate characterisation in metallic systems by small-angle X-ray or neutron scattering, Comptes Rendus Phys. 13 (2012) 246–256. doi:10.1016/j.crhy.2011.12.008.

[22] A. Deschamps, F. De Geuser, Quantitative characterization of precipitate microstructures in metallic alloys using small-angle scattering, (2013). doi:10.1007/s11661-012-1435-7.

[23] C. Fabrice, Small angle neutron scattering, EPJ web of conferences 104, 01004 (2015). doi: 10.1051/epjconf/201510401004.

[24] F. Sun, D. Laillé, T. Gloriant, Thermal analysis of the ω nanophase transformation from the metastable β Ti-12Mo alloy, J. Therm. Anal. Calorim. 101 (2010) 81–88. doi:10.1007/s10973-010-0713-0.

[25] M.A. Hill, D.H. Polonis, Influence of beta phase decomposition on the temperature coefficient of resistivity of titanium alloys, J. Mater. Sci. 22 (1987) 2181–2184. doi: 10.1007/BF01132957.

[26] N.G. Jones, R.J. Dashwood, D. Dye, M. Jackson, Thermomechanical processing of Ti-5Al-5Mo-5V-3Cr, Mater. Sci. Eng. A. 490 (2008) 369–377. doi:10.1016/j.msea.2008.01.055.

[27] H. Seiner, P. Sedl, M. Landa, J. Smilauerov, B. Denand, M. Dehmas *et al.*, On the complementarity between resistivity measurement and ultrasonic measurement for in-situ characterization of phase transitions in Ti-alloys, J. Alloys Compd. 762 (2018) 868–872. doi:10.1016/j.jallcom.2018.05.173.

[28] A. Settefrati, E. Aeby-Gautier, M. Dehmas, G. Geandier, B. Appolaire, S. Audion *et al.*, Precipitation in a near beta titanium alloy on ageing: Influence of heating rate and chemical composition of the beta-metastable phase, Solid State Phenom. 172–174 (2011) 760–765. doi:10.4028/www.scientific.net/SSP.172-174.760.

[29] Q. Contrepois, M. Carton, J. Lecomte-Beckers, Characterization of the β phase decomposition in Ti-5Al-5Mo-5V-3Cr at slow heating rates, Open J. Met. 01 (2011) 1–11. doi:10.4236/ojmetal.2011.11001.

[30] M.J. Donachie, Titanium a technical guide. second ed. Materials Park, OH: ASM International, 2000.

[31] P. Manda, V. Singh, U. Chakkingal, A.K. Singh, Development of α precipitates in metastable Ti-5Al-5Mo-5V-3Cr and similar alloys, Mater. Charact. 120 (2016) 220–228. doi:10.1016/j.matchar.2016.09.005.

[32] ISIS Neutron and Muon Source UK, ENGIN-X Furnace. https://www.isis.stfc.ac.uk/Pages/ENGINX-Furnace.aspx, 2010 (accessed 01 July 2020).

[33] O. Arnold, J.C. Bilheux, J.M. Borreguero, A. Buts, S.I. Campbell, L. Chapon *et al.*, Nuclear instruments and methods in physics research a Mantid — Data analysis and visualization package for neutron scattering and μ SR experiments, Nucl. Inst. Methods Phys. Res. A. 764 (2014) 156–166. doi:10.1016/j.nima.2014.07.029.

[34] P. Zháňal, P. Harcuba, M. Hájek, B. Smola, J. Stráský, J. Šmilauerová *et al.*, Evolution of ω phase during heating of metastable β titanium alloy Ti–15Mo, J. Mater. Sci. 53 (2018) 837–845. doi:10.1007/s10853-017-1519-2.

[35] B. Roebuck, D. Cox, R. Reed, The temeperature dependence of γ' volume fraction in a Ni-based single crystal superalloy from resistivity measurements,Scr. Mater. 44 (2001) 917–921. doi: 10.1016/S1359-6462%2800%2900662-X.

[36] B. Roebuck, M.G. Gee, M. Brooks, D.Cox, R.Reed, Miniature multiproperty tests at elevated temperatures, Int. Conf. Component Optimistion from Materials Properties and Simulation Software, IRC Swansea, Wales, April (1999).

[37] C.A. Schneider, W.S. Rasband, K.W. Eliceiri, NIH Image to ImageJ : 25 years of image analysis, Nat. Methods. 9 (2012) 671–675. doi:10.1038/nmeth.2089.

[38] J. Gao, A.J. Knowles, D. Guan, W.M. Rainforth, ω phase strengthened 1.2GPa metastable β titanium alloy with high ductility, Scr. Mater. 162 (2019) 77–81. doi:10.1016/j.scriptamat.2018.10.043.

[39] P. Zháňal, P. Harcuba, J. Šmilauerová, J. Stráský, M. Janeček, B. Smola *et al.*, Phase transformations in Ti-15Mo investigated by in situ electrical resistance, Acta Phys. Pol. A. 128 (2015) 779–782. doi:10.12693/APhysPolA.128.779.

[40] D. De Fontaine, N.E. Paton, J.C. Williams, The omega phase transformation in titanium alloys as an example of displacement controlled reactions, Acta Metall. 19 (1971) 1153–1162. doi:10.1016/0001-6160(71)90047-2.

[41] J. Nejezchlebová, M. Janovská, H. Seiner, P. Sedlák, M. Landa, J. Šmilauerová *et al.*, The effect of athermal and isothermal ω phase particles on elasticity of β-Ti single crystals, Acta Mater. 110 (2016) 185–191. doi:10.1016/j.actamat.2016.03.033.

[42] J.C. Williams, B.S. Hickman, H.L. Marcus, The effect of omega phase on the mechanical properties of titanium alloys, Metall. Trans. 2 (1971) 1913–1919. doi:10.1007/BF02913423.

[43] J. Debuigne, F. Prima, Growth kinetic model for isothermal omega phase particles in low-cost beta titanium Ti–6.8Mo–4.5Fe–1.5Al alloy, Mater. Trans. 46 (2005) 1433–1435. doi:10.2320/matertrans.46.1433.

[44] T. Gloriant, G. Texier, F. Sun, I. Thibon, F. Prima, J.L. Soubeyroux, Characterization

of nanophase precipitation in a metastable β titanium-based alloy by electrical resistivity, dilatometry and neutron diffraction, Scr. Mater. 58 (2008) 271–274. doi:10.1016/j.scriptamat.2007.10.007.

[45] S.E. Haghighi, H.B. Lu, G.Y. Jian, G.H. Cao, D. Habibi, L.C. Zhang, Effect of α″ martensite on the microstructure and mechanical properties of beta-type Ti-Fe-Ta alloys, Mater. Des. 76 (2015) 47–54. doi:10.1016/j.matdes.2015.03.028.

[46] Y.Q. Wang, S. Clark, V. Janik, R.K. Heenan, D. Alba Venero, K. Yan *et al.*, Investigating nano-precipitation in a V-containing HSLA steel using small angle neutron scattering, Acta Mater. 145 (2018) 84–96. doi:10.1016/j.actamat.2017.11.032.

[47] SasView, SasView user documentation. http://www.sasview.org/docs/user/user.html, 2018 (accessed 01 July 2020).

[48] J. Coakley, A. Radecka, D. Dye, P.A.J. Bagot, H.J. Stone, D.N. Seidman *et al.*, Isothermal omega formation and evolution in the beta-Ti alloy Ti-5Al-5Mo-5V-3Cr, Philos. Mag. Lett. 96 (2016) 416–424. doi:10.1080/09500839.2016.1242877.

[49] Q. Hui, X. Xue, H. Kou, M. Lai, B. Tang, J. Li, Kinetics of the ω phase transformation of Ti-7333 titanium alloy during continuous heating, J. Mater. Sci. 48 (2013) 1966–1972. doi:10.1007/s10853-012-6962-5.

[50] F. Lourdjane, A.A. Raho, Precipitation kinetics of the GP zones in Al4,65at .% Ag(15%Wt.), Am. J. Mater. Sci. Eng. 3 (2015) 11–14. doi:10.12691/ajmse-3-1-3.

[51] I. Sinha, R.K. Mandal, Avrami exponent under transient and heterogeneous nucleation transformation conditions, J. Non. Cryst. Solids. 357 (2011) 919–925. doi:10.1016/j.jnoncrysol.2010.11.005.

[52] I. Sinha, R.K. Mandal, Isothermal nanocrystallization kinetics during polymorphic transformation, J. Non. Cryst. Solids. 355 (2009) 361–367. doi:10.1016/j.jnoncrysol.2008.12.006.

[53] A.D. Abramenkov, Y.M. Fogel, V. V Slyozov, L. V Tanatarov, O.P. Ledenyov, Research on diffusion of Mo substrate atoms into Ti and Cr thin films by secondary ion-ion emission method, Phys. Met. Metallogr. 29 (1970) 4–6. doi: abs/1209.4750.

[54] C.F. Yolton, F.H. Froes, R.F. Malone, Alloying element effects in metastable beta titanium alloys, Met. Trans. A. 10A (1979) 132–134.

[55] K. Hua, J. L. M. Sun, B. Tang, H. Kou, Phase transfrmation during isothermal heat treatment in β-quenched Ti–7Mo–3Nb–3Cr–3Al alloy, Proc. 13th World Conf. Titan. (2016) 605–613.